HOMOGENIZATION AND μCT ANALYSIS FOR THE TRABECULAR BONE REMODELLING

Claudia Chan Yone, Jean-Louis Milan, Jean-Marie Rossi, Jean-François Witz, Mathias Brieu, Patrick Chabrand

Homogenization and μCT analysis for the trabecular bone remodeling

Claudia Chan Yone, Jean-Louis Milan, Jean-Marie Rossi, Jean-François Witz, Mathias Brieu, Patrick Chabrand

February 23, 2012

1 Introduction

Osteoporosis is a bone disease characterized by low bone mass but also a degradation of cancellous bone micro-architecture. Bone weakness can generate fracture, that is why tools have been developed to assess probability of fracture. The clinical device DEXA, is a quantitative measure of bone mineral density (result is a T-score), while FRAX® (1) is a questionary based on statistical analysis including criteria like age, bone mass index and lifestyle. Although those informations are essential in fracture assessment, one in two person undeclared osteoporotic according to WHO definition (T-score < -2.5) will have a fracture (2; 3; 4; 5). That is why bone quantity, or statistical analysis are unsufficient to predict bone weakness, but bone quality i.e bone micro-structure should be considered.

Many numerical models have been developed in purpose to predict bone alteration and so fracture assessment. Bone alteration is due to an imbalance in the bone remodeling process : quantity of new deposited tissue is smaller than the removal old matrix tissue. Furthermore, bone is well known to adapt its morphology to the mechanical environment. From those observations many researchers developed numerical models based on biological and/or mechanical criteria (6; 7; 8; 9; 10; 11; 12; 13). Among those theoritical approachs, some authors worked on real cancellous bone micro-architecture alteration (14; 15; 16; 17; 18). They have simulated

trabecular plate perforation, decrease of bone volume fraction and loss of mechanical properties which can lead to bone fracture. Those approachs are interesting because they used real human bone, and predicted realistic altered cancellous micro-structure due to aging or disease.

Those models used micro-finite element analysis (μFEA) based on 3-D reconstruction from micro-computed tomography acquisition (μCT). Voxels are directly convert in finite elements, as a consequence models are composed of several millions of elements (until 20 millions). The quantity of degree of freedom is not compatible with an iterative process in order to consider biological or mechanical stimuli changes. That is why alteration was randomly distributed over trabeculae and consider not any mechanical criteria. However mechanical environment play a crucial role in activation (19) and localization of bone remodeling : indeed damage and cracks are generally used as precusors of bone remodeling (20; 21; 22; 23).

In this study we will present a method to build μFE model from μCT acquisition reducing degree of freedom in order to simulate bone degradation with an iterative process, so that to integrate mechanical stimuli variations (bed-ridden case), or biological modifications (medical treatment). We will study what is the influence of reducing model complexity in term of mechanical global and local behaviour. Furthermore we will investigate if material heterogenities, like hypermineralized bone, influence repartition of areas which are over or under-constrained among the structure. Indeed, hypermineralized bone is a privileged place of cracks accumulation (24), and can play an important role in ordre to identify remodeling sites.

2 Materials and methods

Trabecular bone sample and μCT imaging

Studied bone is a human femoral head collected behind a femoral neck fracture. The willing donor, was a woman aged of 87 years old, her bone mass index was 19.8 (limit underweight ≤ 18.5) and was prone to bone weakness because she fractured her shoulder in the past.

A cubic specimen was harvested (10x10x10mm) from femoral head and prepared removing marrow with a water bath (37°C) containing a stirring rod. Remaining marrow was extracted with compressed air. Sample was scanned by a μCT system (model Skyscan 1172) at 20μm

resolution. Cross-section images were stored in 16-bit format (format tif) with 1000x1000 pixels in size. Phantoms of cortical and trabecular bone were placed under the sample with respectively a density of hydroxyapatite of 1750 and 800mg/cm^3, *i.e* a physical density of 2.17 and 1.53g/cm^3. These latters gave us a grayscale reference to identify material component and so mechanical properties. Some morphologic datas were computed directly after acqusition by the sofware SKYSCAN CTANalyser (table 1).

BV/TV (%)	**BS/BV (mm^{-1})**	**SMI**	**Tb,Th** (mm)	**Tb,N** (mm^{-1})	**Tb,Sp** (mm)	**DA**
29.87	10.18	0.69	0.343	0.869	0.769	0.677

BV/TV : Bone Volume/ Total Volume; BS/BV : Bone Surface/Bone Volume; SMI : Structure Model Index
Tb,Th : Trabeculae Thickness; Tb,N : Trabeculae Number; Tb,Sp : Trabeculae Space; DA : Degree of Anisotropy

Table 1: Morphometric parameters computed after μCT acquisition

Homogenization/Coarsening method

For the numerical study a central cubical sub-volume equivalent to 4x4x4mm (200x200x200 voxels) was extracted. A coarsening method (25; 26) was applied on the whole volume containing both marrow and bone tissue elements : figure 1 describe the principle in two dimensions : initial voxels of 20x20μm^2 were grouped to new voxels of 40x40μm^2 until 100x100x100μm^2. Initial micro-structure is showed in 3 dimensions without marrow voxels in figure 2(a), and figure 2(c) to figure 2(f) illustrate different case of coarsened voxel. This method allows to simulate degradation of system acquisition, but also to reduce numbers of voxels contained in studied volume.

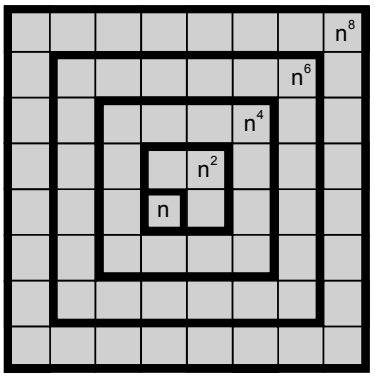

Figure 1: Principle of coarsening in two dimensions : n^m contain m x m voxels of 20μm

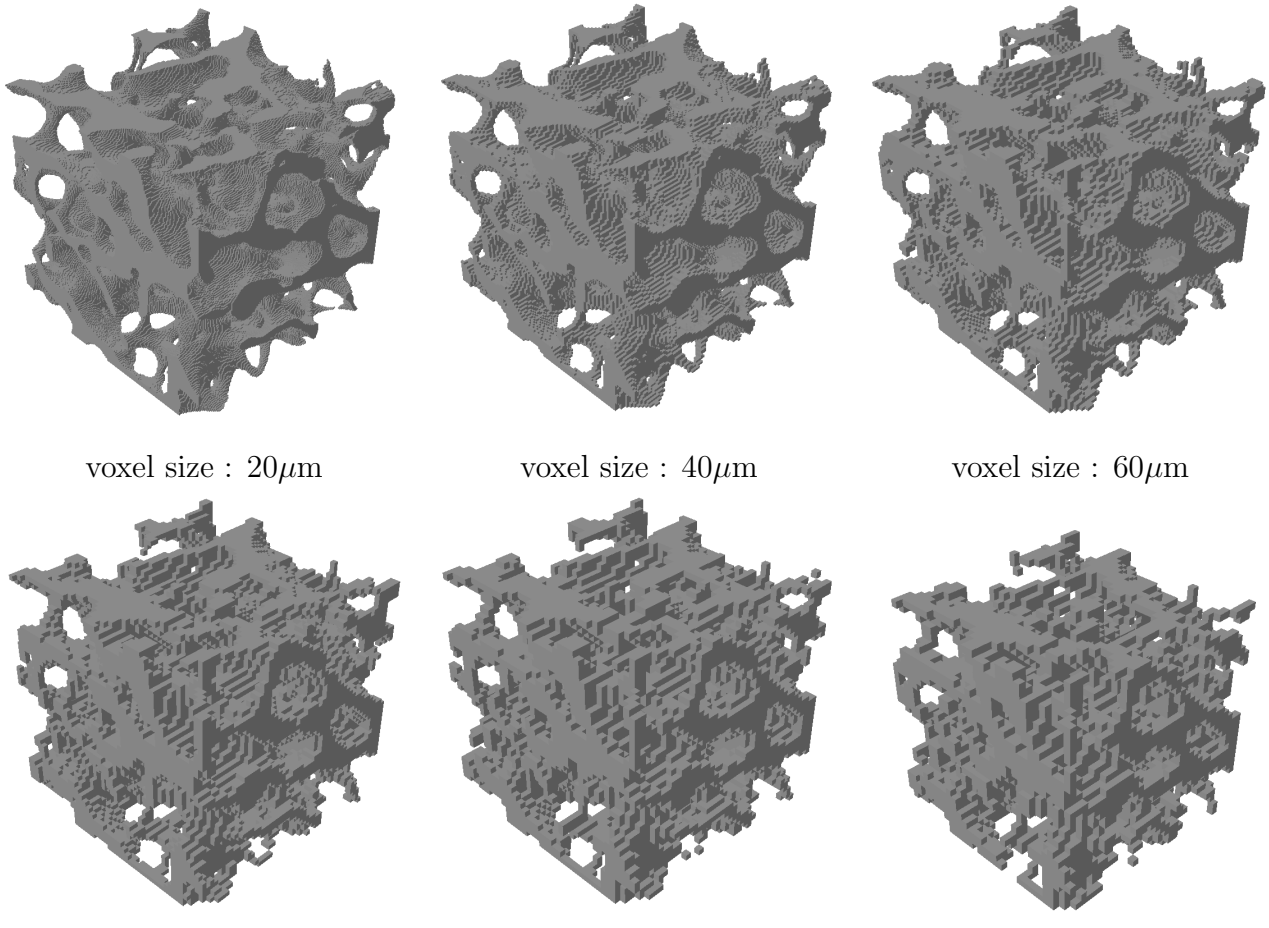

voxel size : 20μm | voxel size : 40μm | voxel size : 60μm

voxel size : 80μm | voxel size : 100μm | voxel size : 120μm

Figure 2: Coarsened models of cancellous bone for different voxel size (sample of 4x4x4mm)

Thresholding and mass computation

Repartition of gray-value of whole volume was plotted (figure 3). Two significant peaks were identified : the highest correspond to the background gray-value (remaining marrow and artefacts), although the smallest correspond to the bone tissue gray-value. Thresholding between background and bone tissue was determined as the middle point between these two peaks. As the black dash-line is cortical phantom gray-value, this graph puts forward the hypermineralized bone : around 70% of bone elements are hypermineralized.

Initial bone mass noted M_0 was computed supposing that element bone mass was linearly correlated to the gray-value element. For coarsened geometry, mass was computed from mass density and also, cortical and trabecular phantom gray-value : each bone mass element was computed and added to get total bone mass. Thresholding was made as sample bone mass was in best agreement with M_0, so as $\frac{|M-M_0|}{M_0} \leq 0.1\%$.

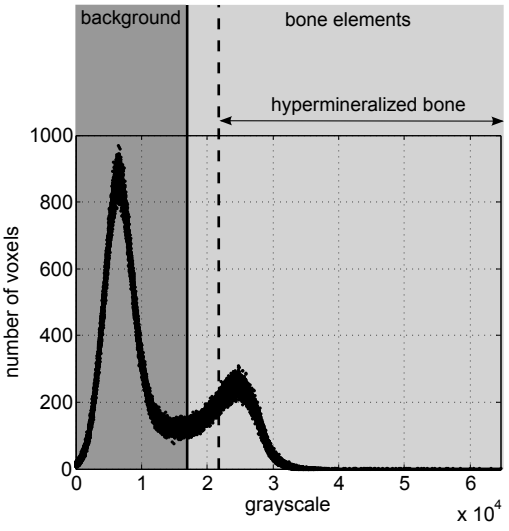

Figure 3: Grayscale of whole reference volume (without coarsening), black solid line is tresholding void/bone and black dotted line is tresholding bone/hypermineralized bone

Material heterogeneous method

Finite element model were generated directly from converting voxels to equally sized eight-node brick elements. All elements are considered elastic linear isotropic. Poisson's ratio was

set to 0.3 and Young Modulus value was calculated with the formula (25) :

$$E_{element} = E_{max}(GV_{element})^{\gamma} \tag{1}$$

where $GV_{element}$ is the normalized gray-value of the element, γ a constant set to 1.5, and E_{max} is the maximal elastic modulus according to maximal gray-value considered and is determined with the equation 2:

$$E_{max} = exp\left(log(E_{cort}) - \gamma log\left(\frac{GV_{cort}}{GV_{max}}\right)\right) \tag{2}$$

where E_{cort} is cortical bone elastic modulus defined by nano-indentation and set to 19GPa (27; 28), GV_{cort} is cortical phantom gray-value, and GV_{max} is maximum gray-value of coarsened volume. E_{cort} was considered as treshold between mineralized and hypermineralized bone because at microscopic scale cancellous and cortical bone elastic modulus are similar (27).
More than 99.9% of bone elements have a Young modulus between 13 and 40GPa, with a maximum at 23GPa (figure 4).

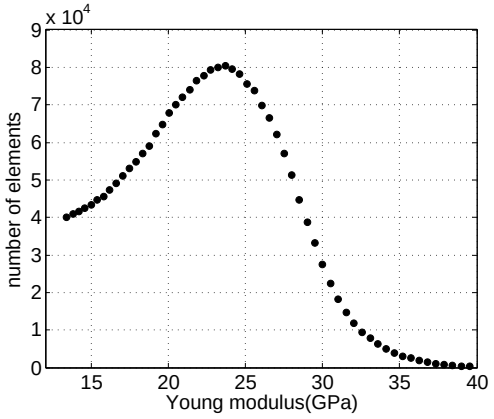

Figure 4: Young modulus distribution taking account of hypermineralized bone for initial voxel size (without coarsening)

Binarization method

As previous method, finite element model were generated directly from converting voxels to

equally sized eight-node brick elements. All elements are considered elastic linear isotropic with a Poisson's ratio was set to 0.3 and Young Modulus set to 19GPa.

Computation and post-processing

Marrow and isolated elements were removed from the finite element analysis. Three static compression tests were simulated with an uniaxial displacement so that global mean strain was equal to -0.3%. Loading was imposed on one face of the sample, on the opposite face displacement along the loading was constrained, furthermore one node was encastred (to avoid part sliding). Reaction force was computed to determine apparent Young modulus of the structure and also strain energy density (directly computed with post-processing Abaqus software).

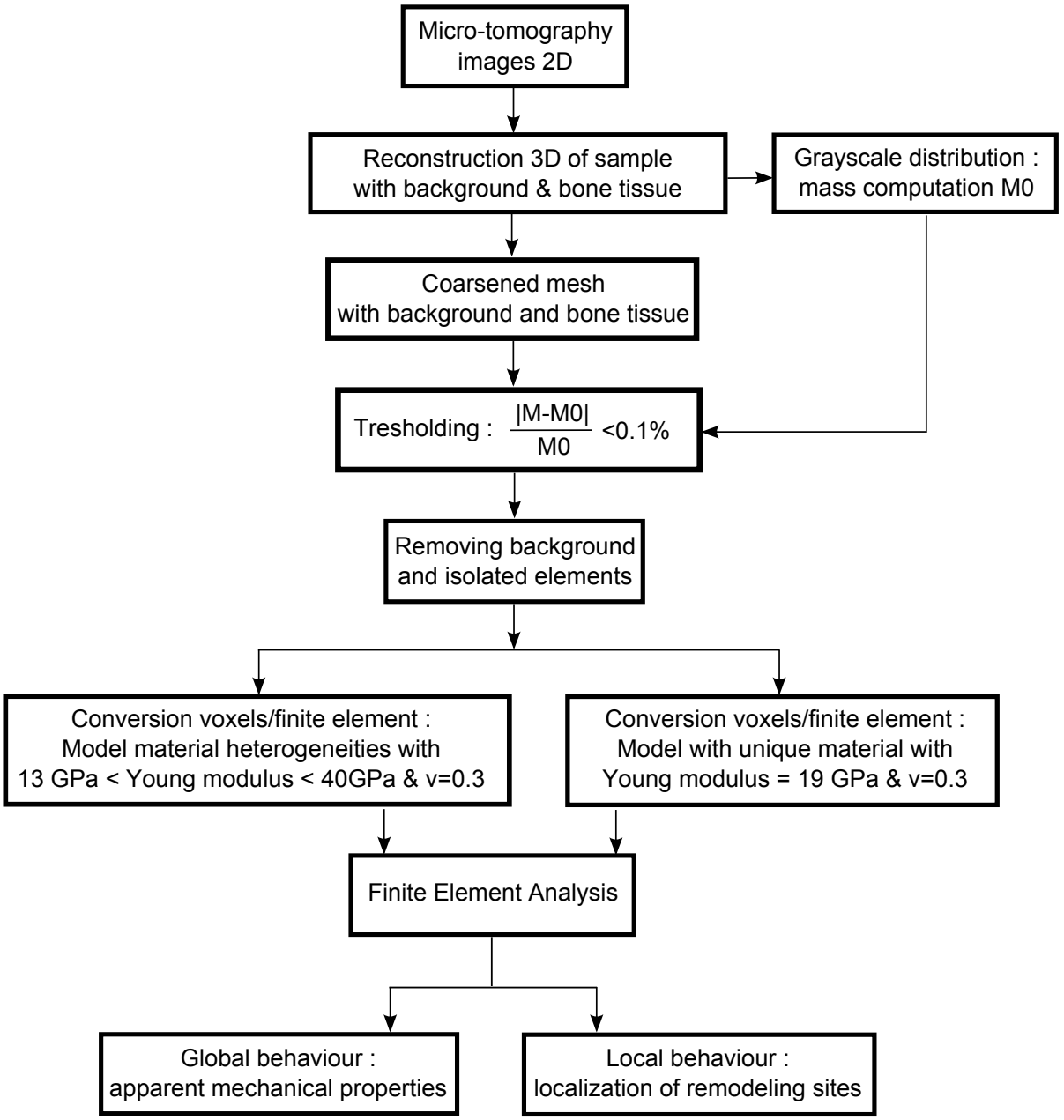

Figure 5: Schematization of method : from micro-tomography acquisition to post-processing of FEA

3 Results

Influence of homogenization

As far as global mechanical behaviour is concerned, apparent Young modulus was computed in 3 principal directions $\overrightarrow{x}$, $\overrightarrow{y}$ and $\overrightarrow{z}$ which correspond to normal sample faces, for different coarsen voxel size. Apparent Young modulus were sorted as $E_3 > E_2 > E_1$, with $E_3 = E_z$, $E_2 = E_x$ and $E_y = E_1$.

Results are plotted in figure 6(a) : for voxel size smaller than 80μm relative apparent Young modulus error is less than 10% compared to the original micro-structure. Relative mean strain energy density error varies from 2.8% to 29.2% respectively for voxel size of 40μm and 100μm (figure 6(b)). Relative error increases significantly from 80μm voxel size.

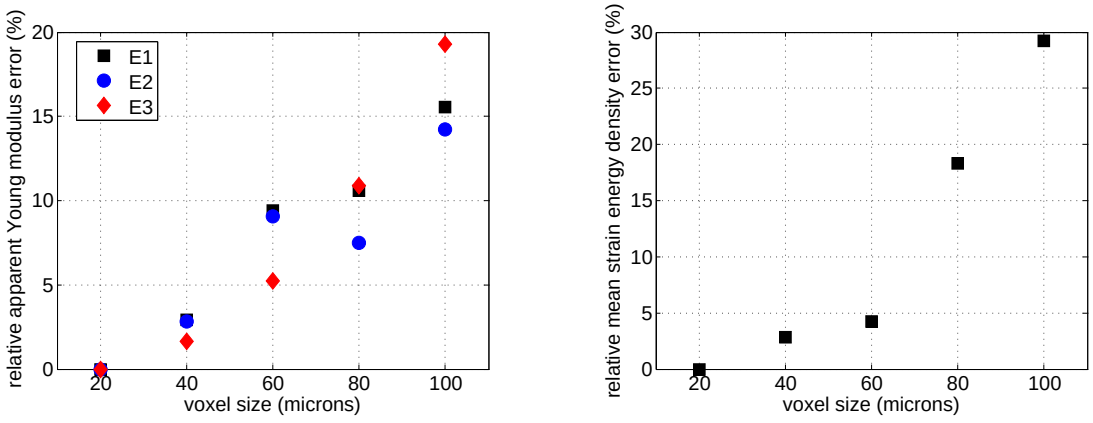

(a) (b)

Figure 6: Relative apparent Young modulus error (a) and relative mean strain energy error (b) computed for coarsened model

As far as local mechanical behaviour is concerned, we compared distribution of strain energy density between initial and coarsen model. Bone tissue where strain exceeds $3000\mu\varepsilon$, which can correpond from a biological point of view to remodeling sites, were identified. Indeed, when strain stimulus is over $3000\mu\varepsilon$ new bone tissue is apposed (29), that is why we focused on hyper-stimulated bone, where strain energy density is over w_{max} defined by :

$$w_{max} = \frac{1}{2} E_{bone} \varepsilon_{max}^2 \quad with \quad E_{bone} = 19GPa, \quad and \quad \varepsilon_{max} = 3000\mu\varepsilon \tag{3}$$

To validate that coarsening method do not degrade localization and volume of remodeling sites, mean distance between remodeling sites was calculated in coarsen model and compared with initial model. Smaller is this value, better is the accuracy of coarsen model. Moreover volume remodeling sites, that is to say bone tissue where strain density exceed $3000\mu\varepsilon$ were compared. As a results, remodeling sites are located in the same place on both coarsen and initial model (figure 7 (a) and (b)). For coarsen voxel of 60 μm, mean distance between remodeling sites is around two voxels, and relative resorbable volume error is low (table 3).

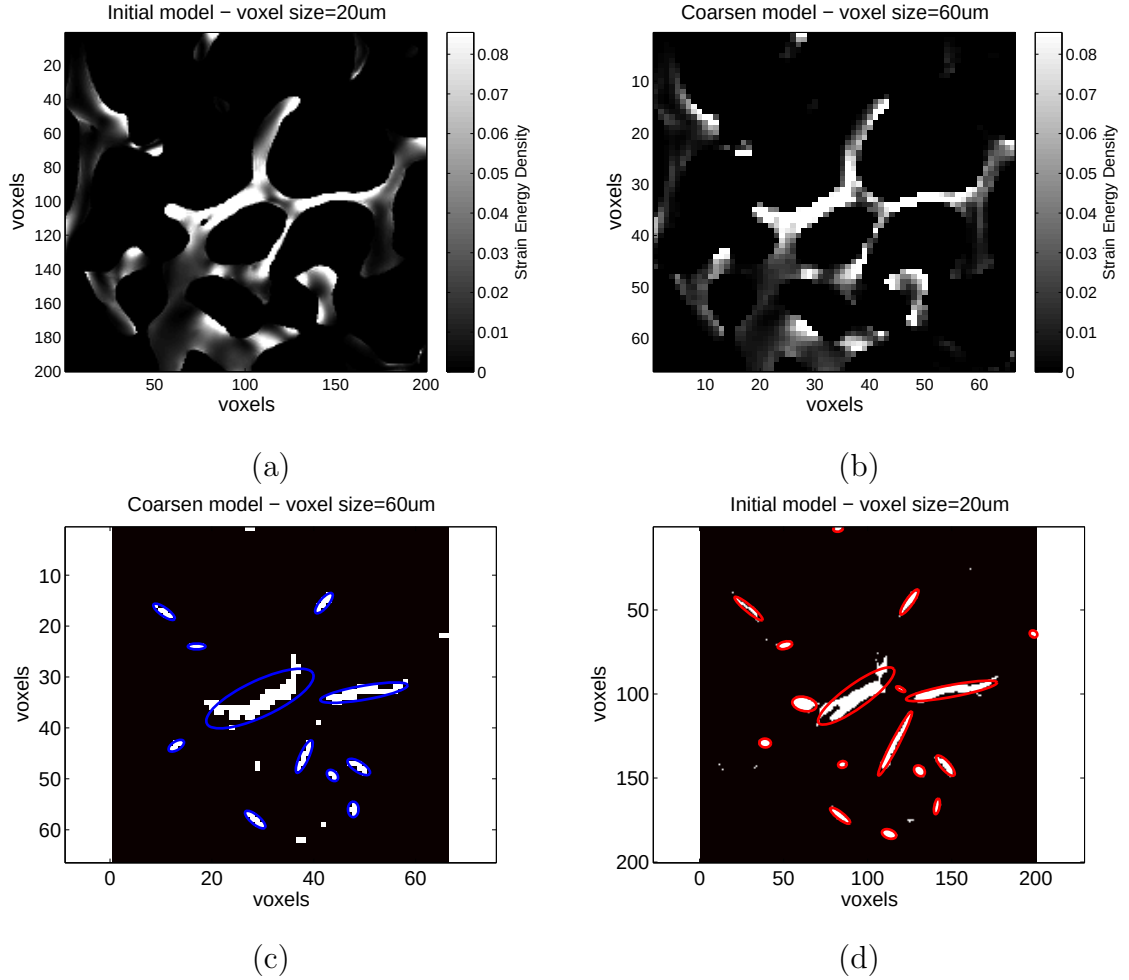

Figure 7: Comparaison of strain energy distribution on initial (a) and coarsen model (b) - Localization of remodeling sites on initial (c) and coarsen model (d)

voxel size (μm)	**number of elements**	**CPU time (sec)**
20	2344910	35927
40	295180	634
60	85336	129
80	36924	44
100	18927	23

Table 2: Number of bone element in finite element analysis and computation time

voxel size (μm)	**maximal Von Mises stress (MPa)**	**relative error mean strain energy density (%)**	**distance remodeling error sites (μm)**	**relative resorbable volume (%)**
20	488.8	0	-	-
40	298.5	2.8	29	0.1
60	185.1	4.2	62	1.4
80	184.3	18.3	199	22.1
100	162.7	29.2	153	27.4

Table 3: Maximal von mises stress and strain energy density for different degree of coarsening

Influence of binarization

Binarized model, generally used in literature, was computed in order to compare influence of material heterogeneities on mechanical behaviour. Mean relative error on apparent Young modulus due to difference of mineralization is 7.5%, which is in agreement with literature (30). Furthermore relative mean strain energy density error is less than 10 % (table 4).

	Heterogeneous model	**Binarized model**
E1 (MPa)	1223	1138
E2 (MPa)	1374	1286
E3 (MPa)	1852	1682
Mean strain energy density (MPa/mm^{-3})	0.0284	0.0257

Table 4: Apparent young modulus and mean strain energy density on heterogeneous and binarized model

Maximum Von mises stress are not exactly similar : 489MPa and 548MPa respectively for heterogeneous and binarized model. Nevertheless this maximum is reached at the same location, which means that structure effect is predominant over material heterogeneities.

From a biological point of view, although number of remodeling sites are same in heterogeneous and binarized model, difference of volume of remodeling sites reachs 19%. So with heterogeneous model remodeling sites are more expanded, which is correlated to material heterogeneities distribution (figure 8). Material heterogeneities do not influence the global mechanical behaviour, nevertheless its influence volume of remodeling sites.

Influence of thresholding

After μCT acquisition, thresolding was made to distinguish background to bone tissue. This step is essential for the rest of the numerical study. Indeed a threshold variation result in variation in bone volume fraction and maximal stiffness (31).

Treshold value was chosen as the middle point between the two significant peaks on grayscale

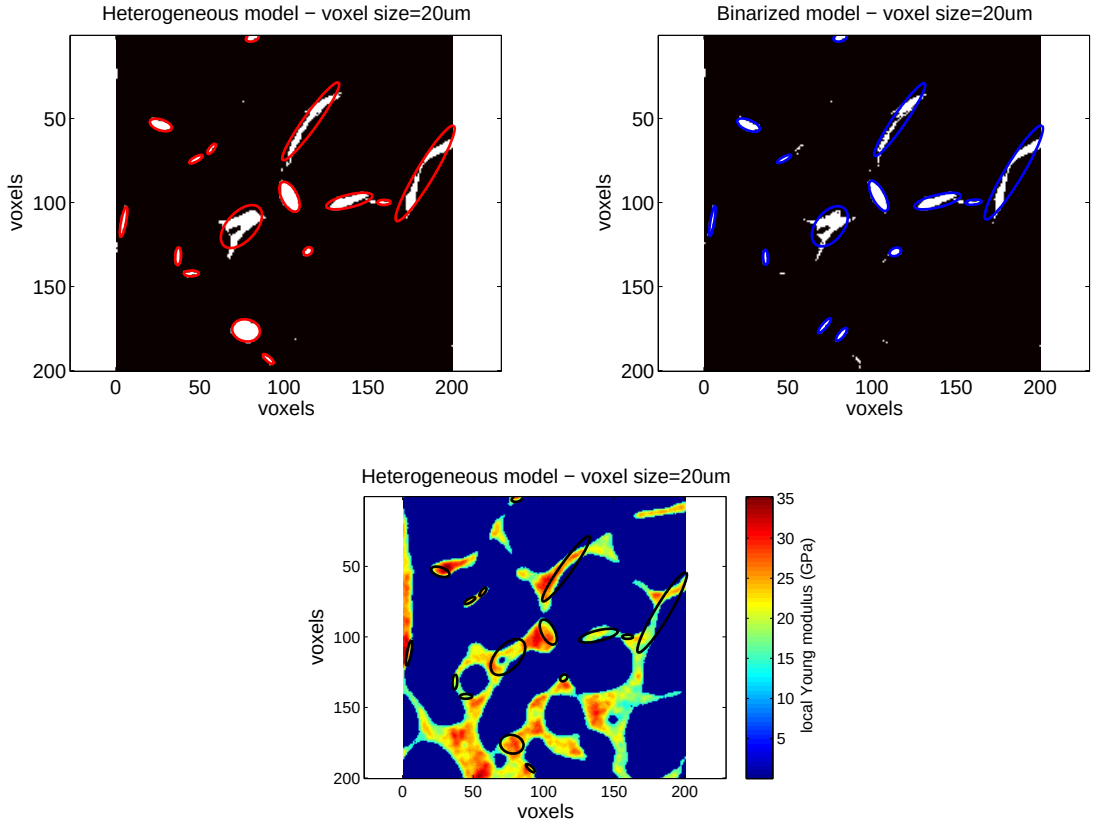

Figure 8: Localization of remodeling sites on heterogeneous and binarized model : sites are located on same place, but more expanded in heterogeneous case which correspond to hyper-mineralized bone tissue (Young modulus¿19GPa)

distribution (figure 3), nevertheless a variation of 5% in tresholding was possible and results in a variation of 5% on bone volume fraction. Higher is coarsen voxel size, higher is the difference in bone volume fraction because voxel volume increases while coarsening (table 5). Moreover many tresholding were made on coarsen models, and a linear relationship was established between apparent Young modulus versus gray-value tresholding (figure 9). Decreasing gray-value treshold consiste in considering thicker trabeculaes and so micro-structure becomes stiffer.

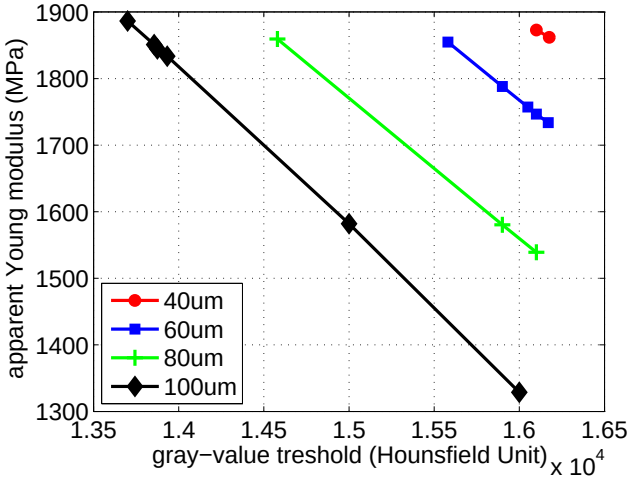

Figure 9: Linear relationship between apparent Young modulus (E3) and gray-value treshold

voxel size (μ**m**)	**Difference in bone volume fraction (%)**	**Difference in apparent Young modulus (%)**
20	3.5	X
40	3.5	6.3
60	4.1	8.6
80	10.3	8.2
100	13.7	9

Table 5: Difference in bone volume fraction and apparent Young modulus for a variation of 5% in tresholding

4 Discussion

Mechanical cancellous bone properties is a decisive parameter in bone fracture. Numerical simulations allow to quantify elastic bone properties during disease or aging (16; 18; 14). Nevertheless those methods use millions of elements and models are not suitable for simulation of iterative process like bone remodeling. So mechanical consideration, like stress concentration, or local mechanical stimulus (inside tissue bone) are not available due to computational cost. In this paper we studied the influence of coarsening voxel size in term of global mechanical behaviour, but also in term of local mechanical behaviour. From micro-tomography acquisi-

tion, we have numerically built new voxels whose gray-value correspond to an average of initial gray-values. This methods allows to increase numerically voxel size, which decrease number of considered elements and degree of freedom for the finite element analysis.

Coarsening voxel size from 20μm (μCT resolution) to 60μm, leads to reduce number of elements from 2 millions to 90000 (for a bone sample of 4x4x4 mm). Furthermore, apparent Young modulus varies from 5%, and computation time which initially goes on 10 hours is reduced to 2 minutes. From a biomechanical point a view, if we are interested in bone remodeling we should compare the agreement of remodeling sites between coarsen and initial model. If we focus on sites where strain exceeds 3000$\mu\varepsilon$, which correspond to the treshold of activation of new bone tissue deposit, we have seen that over-constrained areas in coarsen and initial model one voxel size away, for a coarsen voxel of 60μm. This difference of localization is negligible at osteoclast scale because during remodeling process, several osteoclasts, which measure until 100μm of diameter, come on trabeculae surface and dig a channel on hundred micrometers on trabeculae bone surface. So a variation of 60μm on remodeling site localization is insignificant.

Compared to binarization method which is largely used in the literature, it was put forward that in a hypermineralized bone tissue, volume of bone where strain energy density is over 3000$\mu\varepsilon$ is under estimated at 19% in a binarized model. Nevertheless binarization give an accurate global mechanical behaviour until coarsen voxel of 60μm. Cancellous bone mechanical properties are more dictated by the micro-structure than local material heterogeneities.

Coarsening method is a relevant method to get mechanical cancellous bone properties, nevertheless, as trabeculae are relatively thin, voxel size is limited in order to keep connectivity and realistic bone morphology. Indeed a trabeculae should be composed of 4 or 5 voxels to be relevant in term of mechanical behaviour (32). A numerical study with a voxel size upper than 80μm is not conceivable in order to simulate realistic case.

As a conclusion, it is now possible to compute cancellous bone mechanical properties of realistic sample (8x8x8mm) with directly coarsened voxel while reducing the computational cost. However, a remodeling process can be planned in order to simulate a physiological case : bone alertation due to a low-loading case (bed-ridden case, microgravity), or bone adaptation due to an overloading case (sport). Lastly, as hypermineralized bone is a privileged place of cracks

concentration, this data can be used as initiator sites of bone remodeling.

References

[1] http://www.shef.ac.uk/FRAX/, "Frax® : Who fracture risk assessment tool,"

[2] J. Pasco, E. Seeman, M. Henry, E. Merriman, G. Nicholson, and M. Kotowicz, "The population burden of fractures originates in women with osteopenia, not osteoporosis," *Osteoporosis International*, vol. 17, pp. 1404–1409, 2006. 10.1007/s00198-006-0135-9.

[3] E. S. Siris, P. D. Miller, E. Barrett-Connor, K. G. Faulkner, L. E. Wehren, T. A. Abbott, M. L. Berger, A. C. Santora, and L. M. Sherwood, "Identification and fracture outcomes of undiagnosed low bone mineral density in postmenopausal women," *JAMA: The Journal of the American Medical Association*, vol. 286, no. 22, pp. 2815–2822, 2001.

[4] P. D. Miller, E. S. Siris, E. Barrett-Connor, K. G. Faulkner, L. E. Wehren, T. A. Abbott, Y.-T. Chen, M. L. Berger, A. C. Santora, and L. M. Sherwood, "Prediction of fracture risk in postmenopausal white women with peripheral bone densitometry: Evidence from the national osteoporosis risk assessment," *Journal of Bone and Mineral Research*, vol. 17, no. 12, pp. 2222–2230, 2002.

[5] S. C. E. Schuit, M. van der Klift, A. E. A. M. Weel, C. E. D. H. de Laet, H. Burger, E. Seeman, A. Hofman, A. G. Uitterlinden, J. P. T. M. van Leeuwen, and H. A. P. Pols, "Fracture incidence and association with bone mineral density in elderly men and women: the rotterdam study," *Bone*, vol. 34, no. 1, pp. 195 – 202, 2004.

[6] C. H. Turner, V. Anne, and R. M. V. Pidaparti, "A uniform strain criterion for trabecular bone adaptation: Do continuum-level strain gradients drive adaptation?," *Journal of Biomechanics*, vol. 30, pp. 555–563, June 1997.

[7] M. Bagge, "A model of bone adaptation as an optimization process," *Journal of Biomechanics*, vol. 33, pp. 1349–1357, Nov. 2000.

[8] R. Huiskes, R. Ruimerman, G. H. Van Lenthe, and J. D. Janssen, "Effects of mechanical forces on maintenance and adaptation of form in trabecular bone," *Nature*, vol. 405, pp. 704–706, June 2000.

[9] T. Adachi, K.-I. Tsubota, Y. Tomita, and S. J. Hollister, "Trabecular surface remodeling simulation for cancellous bone using microstructural voxel finite element models," *Journal of Biomechanical Engineering*, vol. 123, pp. 403–409, Oct. 2001.

[10] C. J. Hernandez, G. S. Beaupré, and D. R. Carter, "A theoretical analysis of the changes in basic multicellular unit activity at menopause," *Bone*, vol. 32, pp. 357–363, Apr. 2003.

[11] R. Huiskes, H. Weinans, H. Grootenboer, M. Dalstra, B. Fudala, and T. Slooff, "Adaptive bone-remodeling theory applied to prosthetic-design analysis," *Journal of Biomechanics*, vol. 20, no. 11-12, pp. 1135–1150, 1987.

[12] J. Martínez-Reina, J. M. García-Aznar, J. Domínguez, and M. Doblaré, "A bone remodelling model including the directional activity of bmus," *Biomechanics and Modeling in Mechanobiology*, vol. 8, pp. 111–127, Mar. 2008.

[13] B. Mulvihill and P. Prendergast, "Mechanobiological regulation of the remodelling cycle in trabecular bone and possible biomechanical pathways for osteoporosis," *Clinical Biomechanics*, vol. 25, no. 5, pp. 491 – 498, 2010.

[14] X. S. Liu, A. H. Huang, X. H. Zhang, P. Sajda, B. Ji, and X. E. Guo, "Dynamic simulation of three dimensional architectural and mechanical alterations in human trabecular bone during menopause," *Bone*, vol. 43, pp. 292–301, Aug. 2008. PMID: 18550463.

[15] R. Müller and P. Rüegsegger, "Analysis of mechanical properties of cancellous bone under conditions of simulated bone atrophy," *Journal of Biomechanics*, vol. 29, pp. 1053–1060, Aug. 1996.

[16] R. Müller, "Long-term prediction of three-dimensional bone architecture in simulations of pre-, peri- and post-menopausal microstructural bone remodeling," *Osteoporosis International*, vol. 16, pp. S25–S35, Aug. 2004.

[17] J. C. Van Der Linden, J. A. N. Verhaar, and H. Weinans, "A three-dimensional simulation of age-related remodeling in trabecular bone," *Journal of Bone and Mineral Research: The Official Journal of the American Society for Bone and Mineral Research*, vol. 16, pp. 688–696, Apr. 2001. PMID: 11315996.

[18] J. C. Van Der Linden, J. A. N. Verhaar, H. A. P. Pols, and H. Weinans, "A simulation model at trabecular level to predict effects of antiresorptive treatment after menopause," *Calcified Tissue International*, vol. 73, pp. 537–544, Dec. 2003.

[19] J. Klein-Nulend, A. Van Der Plas, C. Semeins, N. Ajubi, J. Frangos, P. Nijweide, and E. Burger, "Sensitivity of osteocytes to biomechanical stress in vitro," *FASEB J.*, vol. 9, no. 5, pp. 441–445, 1995.

[20] D. B. Burr, R. Martin, M. B. Schaffler, and E. L. Radin, "Bone remodeling in response to in vivo fatigue microdamage," *Journal of Biomechanics*, vol. 18, no. 3, pp. 189–200, 1985.

[21] L. McNamara and P. J. Prendergast, "Bone remodelling algorithms incorporating both strain and microdamage stimuli," *Journal of Biomechanics*, vol. 40, no. 6, pp. 1381–1391, 2007.

[22] S. Ramtani and M. Zidi, "A theoretical model of the effect of continuum damage on a bone adaptation model," *Journal of Biomechanics*, vol. 34, pp. 471–479, Apr. 2001.

[23] M. Doblaré and J. García, "Anisotropic bone remodelling model based on a continuum damage-repair theory," *Journal of Biomechanics*, vol. 35, pp. 1–17, Jan. 2002.

[24] E. G. Vajda and R. D. Bloebaum, "Age-related hypermineralization in the female proximal human femur," *The Anatomical Record*, vol. 255, pp. 202–211, June 1999.

[25] J. Homminga, R. Huiskes, B. Van Rietbergen, P. Rüegsegger, and H. Weinans, "Introduction and evaluation of a gray-value voxel conversion technique," *Journal of Biomechanics*, vol. 34, no. 4, pp. 513–517, 2001.

[26] D. Ulrich, B. Van Rietbergen, H. Weinans, and P. Rüegsegger, "Finite element analysis of trabecular bone structure: a comparison of image-based meshing techniques," *Journal of Biomechanics*, vol. 31, no. 12, pp. 1187 – 1192, 1998.

[27] C. H. Turner, J. Rho, Y. Takano, T. Y. Tsui, and G. M. Pharr, "The elastic properties of trabecular and cortical bone tissues are similar: results from two microscopic measurement techniques," *Journal of Biomechanics*, vol. 32, no. 4, pp. 437 – 441, 1999.

[28] T. Hoc, L. Henry, M. Verdier, D. Aubry, L. Sedel, and A. Meunier, "Effect of microstructure on the mechanical properties of haversian cortical bone," *Bone*, vol. 38, no. 4, pp. 466–474, 2006.

[29] H. M. Frost, "On our age-related bone loss: Insights from a new paradigm," *Journal of Bone and Mineral Research*, vol. 12, no. 10, pp. 1539–1546, 1997.

[30] R. M. Zebaze, A. C. Jones, M. G. Pandy, M. A. Knackstedt, and E. Seeman, "Differences in the degree of bone tissue mineralization account for little of the differences in tissue elastic properties," *Bone*, vol. 48, pp. 1246–1251, June 2011.

[31] T. Hara, E. Tanck, J. Homminga, and R. Huiskes, "The influence of microcomputed tomography threshold variations on the assessment of structural and mechanical trabecular bone properties," *Bone*, vol. 31, pp. 107–109, July 2002.

[32] G. T. Charras and R. E. Guldberg, "Improving the local solution accuracy of large-scale digital image-based finite element analyses," *Journal of Biomechanics*, vol. 33, pp. 255–259, Feb. 2000.